/N-20

/36217

P.14

Numerical Study of Cathode Emission Constraints on Cylindrical Self-Field MPD Thruster Performance

Michael R. LaPointe
Sverdrup Technology, Inc.
Lewis Research Center Group
Brook Park, Ohio

January 1993

NASA
National Aeronautics and
Space Administration

(NASA-CR-190795)   NUMERICAL STUDY
OF CATHODE EMISSION CONSTRAINTS ON
CYLINDRICAL SELF-FIELD MPD THRUSTER
PERFORMANCE Final Report   (Sverdrup
Technology)   14 p

N93-15370

Unclas

G3/20   0136217

NUMERICAL STUDY OF CATHODE EMISSION CONSTRAINTS
ON CYLINDRICAL, SELF-FIELD MPD THRUSTER PERFORMANCE

Michael R. LaPointe
Sverdrup Technology, Inc.
2001 Aerospace Parkway
Brook Park, OH   44142
(216) 977-7453

Abstract

A stability equation relating thruster discharge current, argon propellant mass flow rate, and electrode geometry has been solved for a variety of cylindrical self-field MPD thruster configurations and discharge currents. Realistic values for cathode emission current densities were used to provide additional constraints on the thruster geometries. A two-dimensional MPD code was employed to provide better estimates of the maximum achievable specific impulse, thrust, and flow efficiency for cases of interest. The model results indicate that long life, cylindrical self-field MPD thrusters operated with argon propellant may not be able to provide specific impulse values in excess of 2100 s. Alternate electrode geometries, applied magnetic fields, and/or low molecular weight propellants may be necessary to achieve higher values of specific impulse.

INTRODUCTION

Nuclear electric propulsion (NEP) has been identified as an attractive option for the low power robotic missions and high power cargo and piloted missions envisioned by the national Space Exploration Initiative (Stone 1992). The magnetoplasmadynamic (MPD) thruster is a robust electric propulsion device with the potential to satisfy these mission requirements. In its basic form, the MPD thruster consists of a cylindrical cathode surrounded by a concentric anode (Figure 1). An arc struck between the electrodes ionizes a gaseous propellant, and the interaction of the arc current with the self-induced magnetic field accelerates the plasma to produce thrust. Steady-state MPD thrusters have been operated at power levels approaching 600 kW$_e$, while pulsed, quasi-steady devices have been operated in the megawatt power range (Sovey and Mantenicks 1988 and Myers *et al.* 1991). The engine is designed to provide low, continuous thrust with specific impulse (I_{sp}) values of 1000 to 5000 s. The ability to scale MPD thrusters in size and power permits an evolutionary approach toward NEP utilization, concurrent with the evolution of space nuclear power systems.
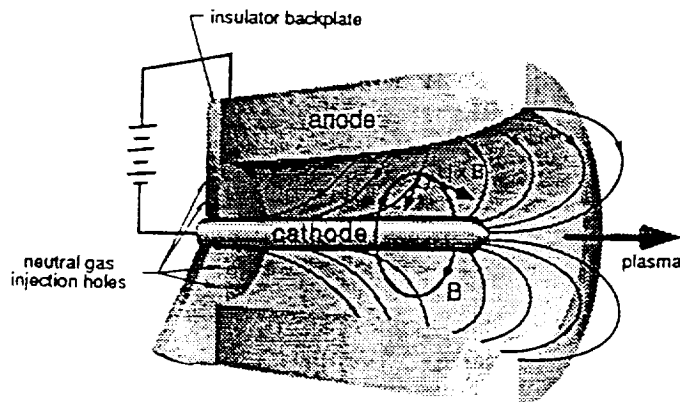

FIGURE 1. Schematic of Self-Field Magnetoplasmadynamic (MPD) Thruster (from Choueiri 1991).

Although simple in design and robust in operation, MPD thruster performance is limited by low thrust efficiency in the operating regimes of interest (Sovey and Mantenieks 1988 and Myers *et al.* 1991). Applied magnetic fields (Myers *et al.* 1991) and flared electrodes (Tahara *et al.* 1987) have been shown to impact MPD thruster efficiency and specific impulse, but for reasons poorly understood at present. Discharge current is sustained by thermionic emission from the cathode, and if not properly sized the evaporation of cathode material leads to limited thruster life (Myers *et al.* 1991). In addition, severe electrode erosion has been observed at higher values of specific impulse, corresponding to the onset of voltage oscillations and unsteady thruster operation. Several mechanisms have been proposed to explain the onset of these instabilities, including anode mass starvation (Hugel 1980), flow choking due to enhanced back-emf (Lawless and Subramaniam 1987 and Subramaniam and Lawless 1988), and the triggering of electrothermal and gradient driven instabilities as the plasma approaches full ionization (Preble 1990, Niewood *et al.* 1990, and Wagner *et al.* 1990). Different operating conditions may trigger one or a combination of the proposed mechanisms, limiting thruster performance and lifetime. On a less dramatic scale, the occurrence of plasma microturbulence has been predicted (Choueiri 1991) and experimentally observed (Choueiri 1991 and Tilley 1991) in MPD thrusters over a range of operating conditions. The presence of microturbulence may enhance the plasma resistivity, resulting in anomalous energy dissipation and a reduction in thruster efficiency.

Numerical Simulation

A 2-D code has been developed at the National Aeronautics and Space Administration (NASA) Lewis Research Center to predict steady-state, self-field MPD thruster performance (LaPointe 1991 and 1992). The numerical simulation is based upon a fully-ionized, single fluid approximation to the MHD equations, including viscous forces, classical plasma transport coefficients, and Hall effects. Maxwell's equations and a generalized form of Ohm's law (which neglects electron pressure gradients) are used to couple the electromagnetic equations to the fluid equations. A single temperature version of the model was used to predict the thrust, plasma voltage, and flow efficiency of cylindrical and flared MPD thruster geometries assuming a fully ionized argon propellant (LaPointe 1991). Thrust predictions agreed with experimentally determined values, and voltage-current predictions followed experimentally observed trends. The model does not simulate electrode falls or microturbulent plasma processes, and the calculated plasma voltage drops were significantly lower than the experimentally measured total discharge voltages.

A more recent version of the code employing separate ion and electron energy equations (LaPointe 1992) has been used to predict the performance of a matrix of cylindrical self-field thruster geometries over a range of operating conditions, again assuming a fully ionized argon propellant. Results of the two-temperature simulations indicate that self-field thruster operation at high specific impulse requires short electrode lengths for stable operation, while longer electrodes are required at low specific impulse to improve thruster flow efficiency. The specific impulse for a self-field MPD thruster is related to $J^2/\dot{m}$, a parameter which is often used to characterize MPD thruster performance (Myers *et al.* 1991). High values of $J^2/\dot{m}$ correspond to predominantly electromagnetic acceleration and higher values of specific impulse, while low values of $J^2/\dot{m}$ correspond to predominantly electrothermal acceleration, and lower values of specific impulse. For reasons not well understood at present, the numerical simulations did not converge for certain combinations of geometry and $J^2/\dot{m}$. Using numerical convergence as a criterion, an equation was formulated which related the maximum stable value of $J^2/\dot{m}$ to the simulated cylindrical thruster geometries:

$$\left(\frac{J^2}{\dot{m}}\right)_c \leq \frac{6.25 \times 10^{10}}{R_c} \left(\frac{L_c}{L_a}\right) \left[5 - \left(\frac{L_a}{R_a}\right) + 4\left(\frac{10R_c - R_a)}{25}\right)\right] \qquad A^2 - s/kg \qquad (1)$$

where J is the discharge current (amps), $\dot{m}$ is the argon propellant mass flow rate (kg/s), and R_a, L_a, R_c and L_c are the anode radius and length and cathode radius and length, respectively, measured in millimeters. The validity of Equation 2 is limited to straight cylindrical electrodes, uniform argon propellant injection at the backplate, $R_c \geq 5$ mm, $R_a \geq 25$ mm, $5 \leq R_a/R_c \leq 10$, $L_a/R_a \leq 5$, and approximately equal electrode lengths ($L_a \simeq L_c$). The onset of thruster instability with increasing $J^2/\dot{m}$ has been observed experimentally, and a comprehensive data base listing maximum $J^2/\dot{m}$ values for a variety of cylindrical thruster geometries was compiled by Preble (1990). The maximum stable $J^2/\dot{m}$ values predicted by Equation 1 were compared to the experimentally determined values of $J^2/\dot{m}$ at onset for thruster geometries which

2

satisfied the constraints associated with Equation 1 (LaPointe 1992). The predicted onset values were within 20% of the experimentally determined values, indicating that Equation 1 could be used to estimate maximum stable $J^2/\dot{m}$ values for cylindrical, self-field thruster geometries subject to the constraints outlined above.

A constraint not previously considered in MPD thruster modeling is the minimum cathode surface area required to support the thruster discharge current via thermionic emission. To sustain cathode integrity over the thousands of hours required for typical low thrust mission profiles, the cathode temperature should be limited to values below approximately 1470 K (Schroff et al. 1981 and Gilland et al. 1990). The corresponding current densities for impregnated tungsten rod cathodes lies between 10 - 20 A/cm^2, the latter value used by Myers et al. (1992) in designing a rod cathode for megawatt MPD thruster applications. For a given discharge current, and assuming uniform thermionic emission from the surface, the minimum required cathode surface area is simply the discharge current divided by the emission current density. For a given cathode radius, the minimum surface area requirement determines a minimum cathode length for use in the numerical simulations. The constraints on cathode surface area, combined with the geometric constraints associated with Equation 1, provide a method to determine the maximum $J^2/\dot{m}$ value consistent with long-life, cylindrical self-field thruster operation.

The maximum $J^2/\dot{m}$ values predicted by Equation 1 are associated with thruster regimes in which electromagnetic body forces provide a substantial fraction of the plasma acceleration, and to a fair approximation the following simple relation may be used to estimate the thruster specific impulse (Jahn 1968):

$$I_{sp} \approx \left[\frac{\mu_0}{4\pi G} \ln \left(\frac{R_a}{R_c} \right) \right] \frac{J^2}{\dot{m}} \quad s \tag{2}$$

where G is the acceleration due to gravity (9.8 m/s^2) and μ_0 is the permeability of free space ($4\pi \times 10^{-7}$). Although the specific impulse will be somewhat higher when thermal acceleration processes are included, the trends in specific impulse obtained by Equation 2 can be used to determine the cylindrical thruster geometries which produce the maximum achievable I_{sp} values for a given discharge current. Once the geometries are identified, a more detailed simulation may be performed using the MHD codes discussed earlier. A simple numerical scheme was thus written to evaluate the maximum $J^2/\dot{m}$ and associated specific impulse values over a range of discharge currents and cylindrical thruster geometries consistent with cathode current density limitations and the geometric constraints associated with Equation 1. The results of this analysis are presented in the section below.

RESULTS

To remain within the constraints imposed by Equation 1, the assumed cathode radii considered in this study were limited to values between 5 mm and 25 mm. The cathode radius in combination with the assumed cathode emission current density and given discharge current provide a minimum required cathode length for each case. Preble (1990) showed that equal electrode lengths offered the greatest self-field thruster stability, hence the anode length was set equal to the cathode length in this analysis. Consistent with the constraints on Equation 1, the anode radius was limited to values between 5 and 10 times the cathode radius, and the electrode lengths were limited to values less than 5 times the anode radius.

A simple numerical scheme was developed to evaluate the critical $J^2/\dot{m}$ and specific impulse values for various emission current densities and total discharge currents, subject to the above geometric constraints. For each emission current density, the minimum cathode surface area required to support a given thruster discharge current was determined. Given a cathode radius, the cathode surface area determined the necessary cathode length and, by default, the anode length of the thruster. The anode radius was then varied from 5 times the cathode radius to 10 times the cathode radius, with the constraint that the ratio of anode length to anode radius was less than 5; if this constraint was not satisfied, the geometry was not evaluated. The cathode radius was varied between 5 mm and 25 mm, the cathode emission current density was varied between 10 and 40 A/cm^2, and the total discharge current was varied from 250 A to 10,000 A. The variations in cathode and anode radii and corresponding variations in electrode lengths provided a matrix of long-life thruster geometries for each combination of cathode emission current density and discharge current. The maximum stable $J^2/\dot{m}$ and specific impulse values were calculated using Equations 1 and 2 for each combination

of emission current density, discharge current, and thruster geometry. The geometry which provided the maximum value of specific impulse for a given emission current density and total discharge current was identified, and the results are listed in Tables 1 through 3 below. It should be noted that the maximum achievable value of specific impulse did not necessarily coincide with the maximum stable value of $J^2/\dot{m}$, due to the geometric coefficient in Equation 2.

Table 1 displays the optimum thruster geometry, critical $J^2/\dot{m}$ value, and maximum achievable I_{sp} for a range of discharge currents assuming a cathode emission current density of 10 A/cm², and Table 2 lists similar parameters for a cathode emission current density of 20 A/cm². It may be possible to increase the emission current density by grooving or texturing the cathode surface, thus providing a higher surface area for thermionic emission (Gilland et al. 1990 and Myers et al. 1991). The effect of increasing the cathode emission current density to 40 A/cm² is shown in Table 3. It should be remarked that although hollow cathodes have shown the potential for sustained MPD thruster operation (Mantenieks and Myers 1992), they are not currently incorporated into MPD thruster simulations due to the added complexity of modeling the hollow cathode discharge physics (Salhi and Turchi 1992), and are not considered in this study.

TABLE 1. Optimum Geometries, Critical $J^2/\dot{m}$, and Maximum I_{sp}
Values for Various Thruster Discharge Currents. Cathode
Emission Current Density = 10 A/cm².

J (A)	R_c (mm)	R_a (mm)	L_c, L_a (mm)	$\left(J^2/\dot{m}\right)_{cr}^a$ (A²-s/kg)	$(I_{sp})_{cr}^b$ (s)	$\dot{m}$ (Ar)^c (kg/s)
250	5	35	80	6.41×10^{10}	1272	1.0×10^{-6}
500	10	50	80	7.13×10^{10}	1171	3.5×10^{-6}
750	15	75	80	6.64×10^{10}	1091	8.5×10^{-6}
1000	15	75	106	6.49×10^{10}	1066	1.54×10^{-5}
1500	15	75	160	6.20×10^{10}	1018	3.63×10^{-5}
2000	20	100	160	6.07×10^{10}	996	6.59×10^{-5}
2500	20	100	200	5.94×10^{10}	976	1.05×10^{-4}
5000	25	125	318	5.61×10^{10}	922	4.46×10^{-4}
7500	25	125	477	5.30×10^{10}	870	1.06×10^{-3}
10000	25	150	637	4.19×10^{10}	766	2.39×10^{-3}

^{a} Critical $J^2/\dot{m}$ corresponding to maximum I_{sp}.
^{b} Maximum value of I_{sp} based on Equation (2).
^{c} Argon propellant, fully ionized.

Based on the critical $J^2/\dot{m}$ value and the discharge current, a minimum propellant mass flow rate for stable operation can be determined, and has been included in the tables. Because the stability relation (Equation 1) was derived under the approximation of fully ionized argon mass flow, there is some concern that the relation breaks down at the lower discharge currents listed in the tables. However, the low mass flow rates associated with these operating conditions ensures that the propellant is sufficiently ionized even at these low discharge currents for the full-ionization approximation to remain valid (Randolph et al. 1992).

4

TABLE 2. Optimum Geometries, Critical $J^2/\dot{m}$, and Maximum I_{sp} Values for Various Thruster Discharge Currents. Cathode Emission Current Density = 20 A/cm^2.

J (A)	R_c (mm)	R_a (mm)	L_c, L_a (mm)	$\left(J^2/\dot{m}\right)^a_{cr}$ (A^2-s/kg)	$(I_{sp})^b_{cr}$ (s)	$\dot{m}$ (Ar)^c (kg/s)
250	5	30	40	8.59×10^{10}	1571	7.30×10^{-7}
500	5	35	80	6.41×10^{10}	1272	3.90×10^{-6}
750	10	50	60	7.38×10^{10}	1212	7.62×10^{-6}
1000	10	50	80	7.13×10^{10}	1171	1.40×10^{-5}
1500	15	75	80	6.64×10^{10}	1091	3.39×10^{-5}
2000	15	75	106	6.49×10^{10}	1066	6.16×10^{-5}
2500	15	75	133	6.35×10^{10}	1042	9.84×10^{-5}
5000	20	105	199	5.94×10^{10}	976	4.21×10^{-4}
7500	25	125	239	5.77×10^{10}	948	9.75×10^{-4}
10,000	25	125	318	5.61×10^{10}	922	1.78×10^{-4}

^{a} Critical $J^2/\dot{m}$ corresponding to maximum I_{sp}.
^{b} Maximum value of I_{sp} based on Equation (2).
^{c} Argon propellant, fully ionized.

TABLE 3. Optimum Geometries, Critical $J^2/\dot{m}$, and Maximum I_{sp} Values for Various Thruster Discharge Currents. Cathode Emission Current Density = 40 A/cm^2.

J (A)	R_c (mm)	R_a (mm)	L_c, L_a (mm)	$\left(J^2/\dot{m}\right)^a_{cr}$ (A^2-s/kg)	$(I_{sp})^b_{cr}$ (s)	$\dot{m}$ (Ar)^c (kg/s)
250	5	30	20	9.42×10^{10}	1722	6.60×10^{-7}
500	5	30	40	8.59×10^{10}	1571	2.91×10^{-6}
750	5	30	60	7.76×10^{10}	1420	7.25×10^{-6}
1000	5	35	86	6.41×10^{10}	1272	1.56×10^{-5}
1500	10	50	60	7.38×10^{10}	1212	3.05×10^{-5}
2000	10	50	80	7.13×10^{10}	1171	5.61×10^{-5}
2500	10	50	100	6.88×10^{10}	1130	9.08×10^{-5}
5000	15	75	133	6.35×10^{10}	1042	3.94×10^{-4}
7500	20	100	150	6.10×10^{10}	1001	9.22×10^{-4}
10,000	20	100	200	5.94×10^{10}	976	1.68×10^{-4}

^{a} Critical $J^2/\dot{m}$ corresponding to maximum I_{sp}.
^{b} Maximum value of I_{sp} based on Equation (2).
^{c} Argon propellant, fully ionized.

Although the specific impulse values do not include a thermal acceleration component, the I_{sp} values listed in Table 1 indicate that, for cathode current densities of 10 A/cm^2, the cylindrical self-field MPD thruster with argon propellant is probably not capable of delivering specific impulse values greatly in excess of 1300 s. Of particular interest, the calculated maximum specific impulse *decreases* with increasing discharge current, due to the effects of the increasing electrode dimensions on the critical $J^2/\dot{m}$ value required for thruster stability, and the logarithmic effect of the electrode radii in the expression for specific impulse. This trend is repeated in Table 2, which indicates that a maximum specific impulse of roughly 1600 s may be achieved with 20 A/cm^2 cathode current densities, and in Table 3, which yields the highest estimated I_{sp} of around 1720 s for a cathode current density of 40 A/cm^2.

The decrease in achievable specific impulse associated with the increase in electrode dimensions is consistent with the results of previous numerical simulations (LaPointe 1992), which predicted that higher specific impulse values could be achieved by thrusters with smaller ratios of R_a/R_C and shorter electrode lengths. The geometries listed in Tables 1 - 3 are the optimum cylindrical self-field thruster geometries which provide the highest specific impulse at the given discharge current, consistent with the constraints on cathode emission current density. To obtain the lower emission current densities associated with long thruster life requires larger cathodes to sustain higher discharge currents, but the larger electrode geometries reduce the stable operating regime (Equation 1) and consequently reduce the achievable specific impulse. Although not addressed in this study, uniform thermionic emission from the cathode surface is unlikely to occur in actual thruster operation. Non-uniform emission may require the use of even larger cathode surface areas to sustain the discharge current and to satisfy the requirements of long-life cathode operation, leading to a further reduction in the achievable specific impulse.

Figure 2 displays the calculated maximum achievable specific impulse as a function of discharge current for the three uniform cathode emission current densities considered in this study. Each of the calculated specific impulse values plotted in the figure corresponds to the model geometry which provided the maximum I_{sp} at each current level, as listed in Tables 1 through 3. The achievable specific impulse falls fairly rapidly with increasing discharge current, then levels off at discharge currents above 5000 A to approximately 900, 1000, and 1100 s for cathode emission current densities of 10, 20 and 40 A/cm^2, respectively.
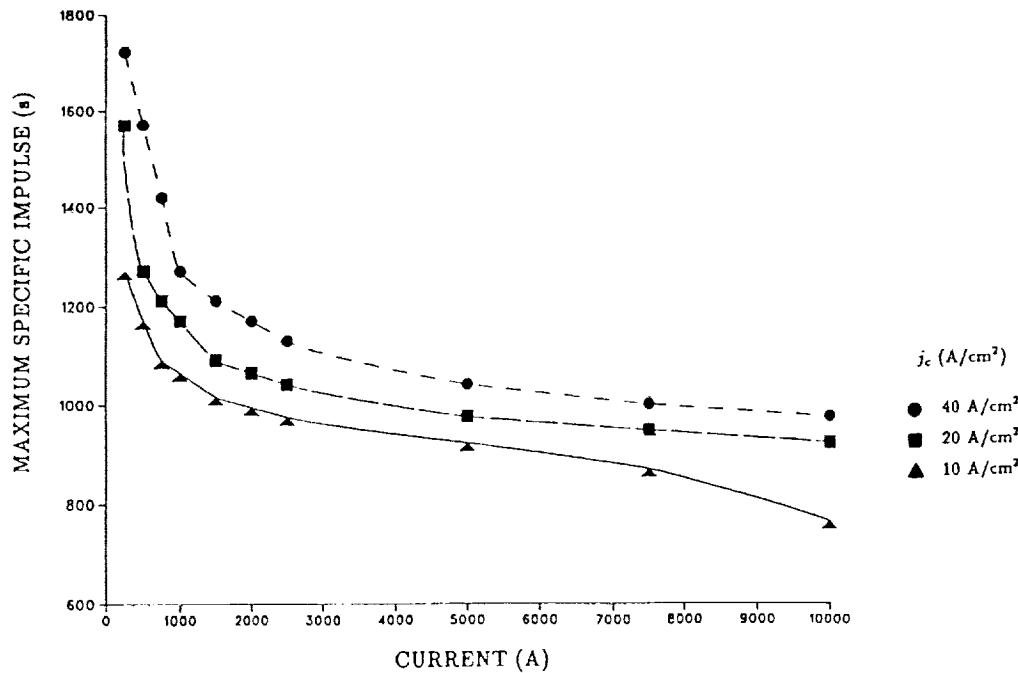

FIGURE 2. Maximum Achievable Specific Impulse, Calculated Using Equation (2).

As noted, the values of achievable specific impulse calculated using Equation 2 do not include contributions due to thermal acceleration, hence a two-temperature MPD model was employed to better estimate thruster performance. The numerical simulations were limited to cases with cathode current densities of 20 A/cm^2 and 40 A/cm^2, due to their higher calculated specific impulse values. Electrode geometries, discharge currents, and propellant mass flow rates were obtained from Tables 2 and 3. Electrode temperatures in the model were set uniformly to 500 K at the anode surface and 1500 K at the cathode surface. Additional information on the MHD equations and the solution technique are discussed by LaPointe (1991 and 1992). Results of the MPD thruster simulations for discharge currents of 250, 500, 1000, 2500, and 5000 A are shown in Figures 3 through 6. Figure 3 displays the predicted specific impulse as a function of discharge current for the two cathode current densities. As expected, the trend toward decreasing specific impulse with increasing discharge current is reproduced. The values of specific impulse predicted by the MPD model are typically 20-30% higher than the values calculated using Equation 2, indicating a fairly modest thermal component to the plasma acceleration. The highest specific impulse achieved for a uniform cathode emission current of 20 A/cm^2 was approximately 1930 s at a discharge current of 250 A. The maximum achievable specific impulse for this case rapidly decreases with increasing discharge current, and levels off at approximately 1350 s for discharge currents between 1000 and 2500 A. As the discharge current is increased to 5000 A, the maximum achievable I_{sp} drops to approximately 1220 s. Increasing the cathode emission current density to 40 A/cm^2 raises the maximum achievable I_{sp} to 2080 s, which again occurs for a discharge current of 250 A. Increasing the discharge current decreases the maximum achievable I_{sp} for stable thruster operation to approximately 1300 s at 2500 A, after which the achievable I_{sp} remains around 1250 s for higher discharge currents. It should be kept in mind that each of the maximum achievable I_{sp} values at each current level are generally associated with different thruster geometries, as noted in the tables.
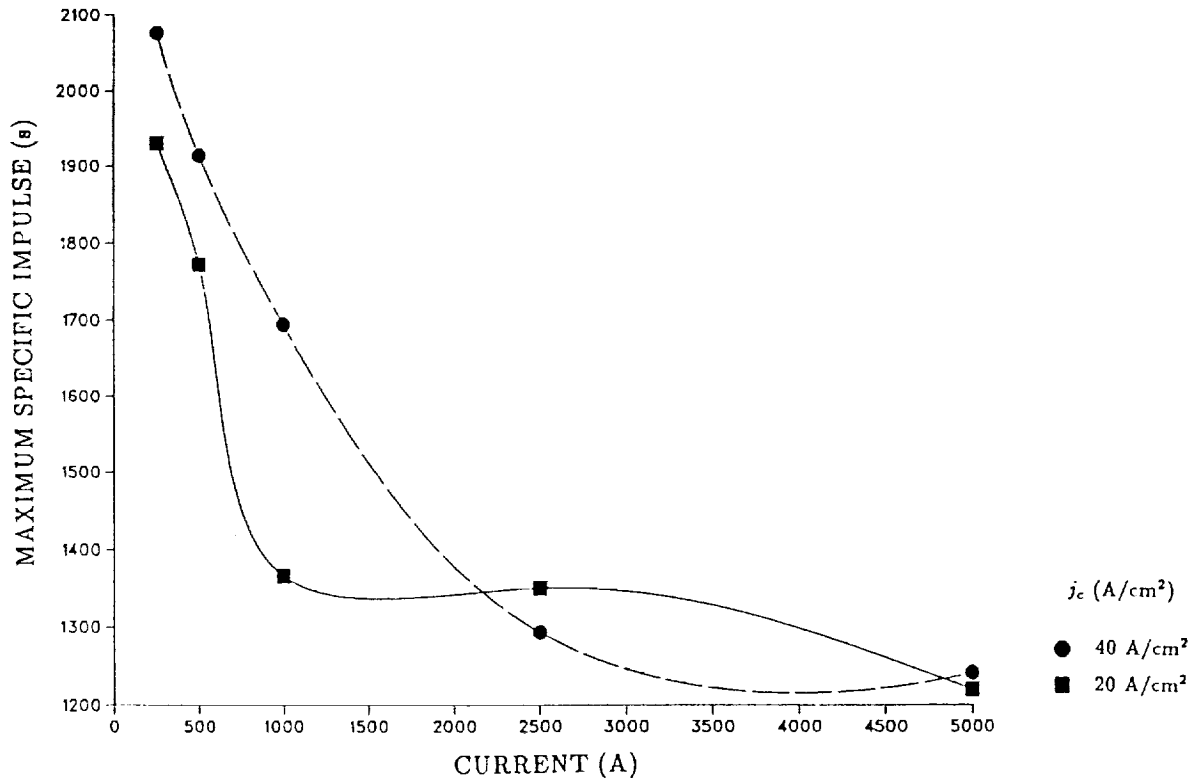

FIGURE 3. Maximum Achievable Specific Impulse, Predicted by MPDT Simulation.

Figure 4 shows the thrust as a function of discharge current and cathode emission current density, as predicted by the two-temperature MPD thruster simulation. The thrust is similar for the 20 A/cm² and 40 A/cm² cathode emission current densities over the range of thruster discharge currents considered. This is not surprising, because at the high $J^2/\dot{m}$ parameters associated with the maximum I_{sp} values, the thrust is primarily due to electromagnetic body forces (Jahn 1968):

$$T(N) = \left[\frac{\mu_o}{4\pi} \ln\left(\frac{R_a}{R_c}\right)\right] J^2 \tag{3}$$

The thrust is thus proportional to the square of the discharge current, multiplied by a geometric factor. Tables 2 and 3 show that the ratios of R_a/R_c at each discharge current are similar, hence the thrust at each discharge current will also be similar. Additional variations in the total thrust at each discharge current are produced by the addition of thermal acceleration processes to the electromagnetic thrust, although these contributions are modest for the cases considered ($\leq$ 25% of the total thrust). Viscous forces, although included in the simulations, were negligible for the cases considered.
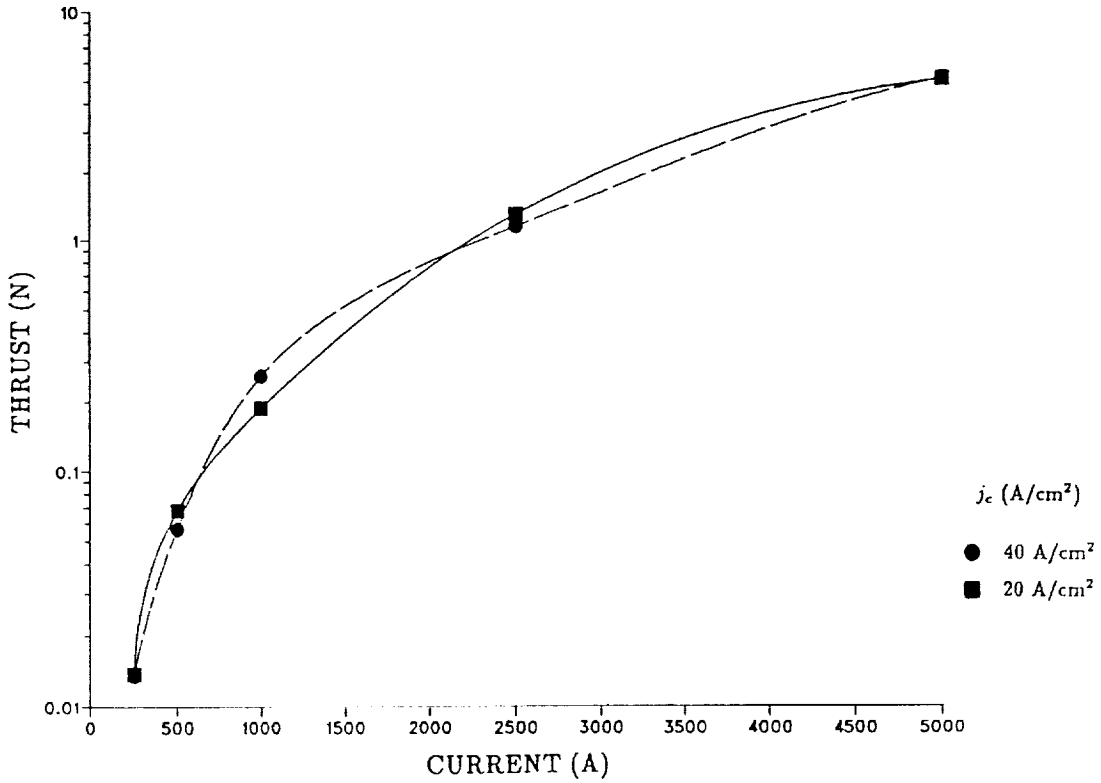

FIGURE 4. Predicted Thrust Associated with Maximum Specific Impulse Values.

Figure 5 shows the calculated plasma fall voltage as a function of discharge current, obtained by integrating the calculated electric field between the electrodes. The MPD simulation does not include electrode effects, hence an estimate of the total discharge voltage cannot be obtained. The voltage trends corresponding to the two cathode emission current densities are similar, showing a nearly linear increase in plasma potential with increasing discharge current. The plasma potential can be used to estimate the power deposited into the plasma, which can then be compared with the thrust power to determine the thruster flow efficiency η_f:

$$\eta_f = \frac{T^2}{2\dot{m}P_p} = \frac{T^2}{2\dot{m}V_pJ} \tag{4}$$

8

where T denotes thrust, P_p is the power deposited into the plasma, V_p is the plasma fall voltage, and J is the discharge current. The total thruster efficiency will be significantly less than the calculated thruster flow efficiency, primarily because of power lost to the thruster electrodes (Myers *et al.* 1991). Nevertheless, the trends in flow efficiency serve to identify regimes of potentially more efficient thruster operation. The flow efficiency as a function of discharge current is plotted in Figure 6 for the cases under investigation. The lowest flow efficiencies occur at the lower discharge currents, which is unfortunate since operation at the lower discharge currents produce the highest calculated values of specific impulse. The lower flow efficiencies result from the shorter electrode lengths associated with the lower discharge currents, and are consistent with previous numerical results (LaPointe 1992). The flow efficiencies generally increase with increasing discharge current, due to an increase in the electrode lengths required to sustain the higher current levels. Thus, while the thruster geometries associated with the lower thruster discharge currents produce the highest achievable values of specific impulse, they are saddled with flow efficiencies which may render them too low to be competitive.
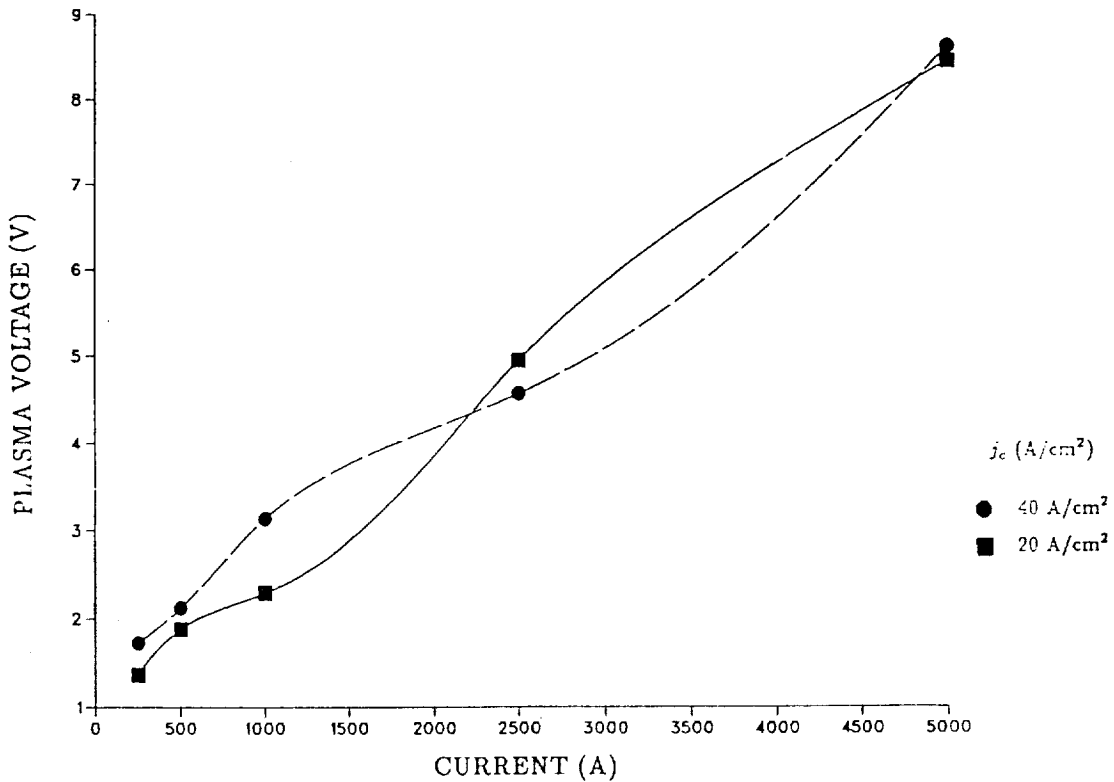

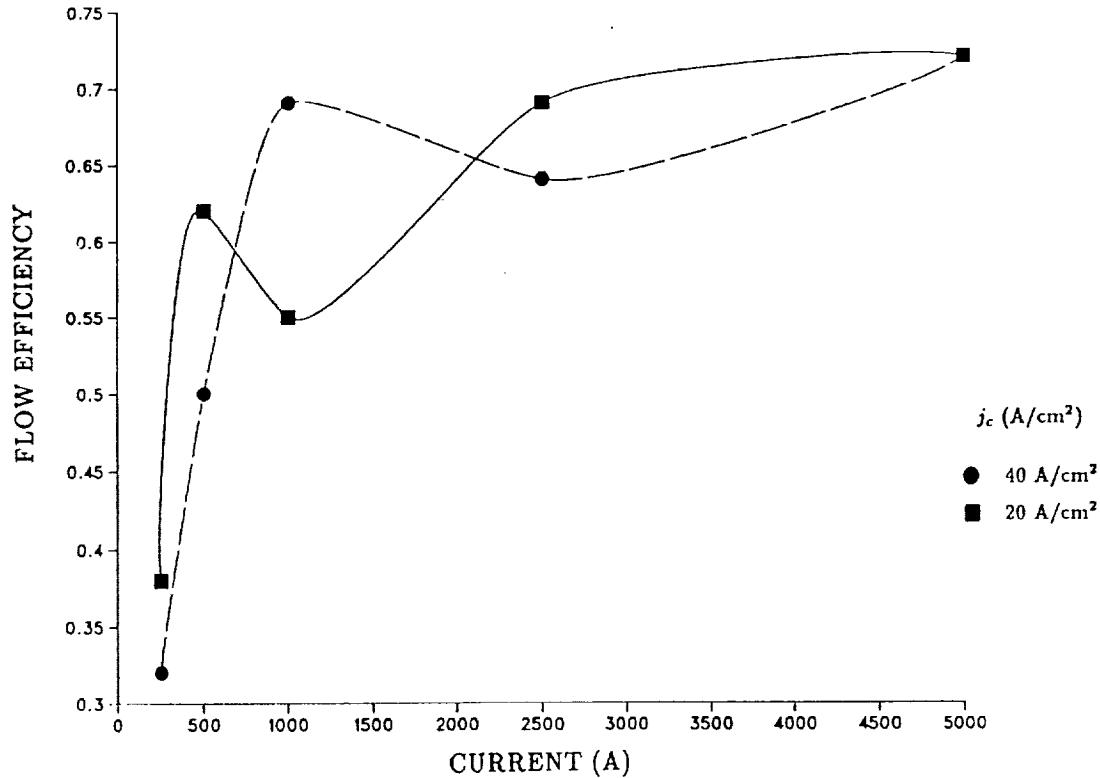FIGURE 5. Predicted Plasma Voltage Associated with Maximum Specific Impulse Values.

FIGURE 6. Predicted Flow Efficiency Associated with Maximum Specific Impulse Values.

CONCLUSIONS

A stability equation relating thruster discharge current, propellant mass flow rate, and electrode geometry has been solved for a variety of cylindrical self-field MPD thruster configurations. A range of uniform cathode emission current densities have been used to provide additional constraints on the thruster geometries. From the stability relation, maximum values of thruster specific impulse and the associated electrode geometries have been determined for several thruster discharge currents. A two-dimensional MPD code was then used to provide better estimates of the specific impulse, thrust, and flow efficiency for cases of interest. Results indicate that cylindrical self-field MPD thrusters operated with argon propellant may not be able to provide specific impulse values in excess of 2100 s. The high specific impulse values are associated with lower values of the thruster flow efficiency, caused by short electrode lengths. Lengthening the electrodes improves the flow efficiency but reduces the maximum achievable specific impulse. Based on these results, it appears unlikely that cylindrical, self-field MPD thrusters operated with argon propellant will provide the necessary combination of specific impulse, efficiency, and lifetime required for missions of interest. Attention should be focused on the use of low molecular weight propellants, alternate electrode geometries, and/or applied magnetic fields to make the MPD thruster a more viable propulsion source for high specific impulse missions.

10

Acknowlededgments

References

Choueiri, E. Y. (1991) Electron-Ion Streaming Instabilities of an Electromagnetically Accelerated Plasma, Ph.D. Dissertation, Department of Mechanical and Aerospace Engineering, Princeton University, Princeton, NJ, October 1991.

Gilland, J. H., R. M. Myers, and M. J. Patterson (1990) "Multimegawatt Electric Propulsion System Design Considerations", AIAA 90-2552, July 1990.

Hugel , H. (1980) "Effect of Self-Magnetic Forces on the Anode Mechanism of a High Current Discharge", *IEEE Trans. Plasma Sci.*, **PS-8**(4): 437-442.

Jahn, R. G. (1968) *Physics of Electric Propulsion*, McGraw-Hill, Inc., New York, pp. 197-253.

LaPointe, M. R. (1991) "Numerical Simulation of Self-Field MPD Thrusters", AIAA 91-2341, June 1991; also see NASA CR-187168, August 1991.

LaPointe, M. R. (1992) "Numerical Simulation of Geometric Scale Effects in Cylindrical Self-Field MPD Thrusters", AIAA 92-3297, July 1992; also see NASA CR-189224, August 1992.

Lawless, J. L. and V. V. Subramaniam (1987) "Theory of Onset in Magnetoplasmadynamic Thrusters", *J. Prop. and Power*, **3**(2): 121-127.

Mantenieks, M. A. and R. M. Myers (1991) "Preliminary Test Results of a Hollow Cathode MPD Thruster", IEPC 91-076, presented at the 22nd International Electric Propulsion Conference, Viareggio, Italy, October 14-17, 1991.

Myers, R. M., M. A. Mantenieks, and M. R. LaPointe (1991) "MPD Thruster Technology", AIAA 91-3568, September 1991; also see NASA TM-105242, September 1991.

Myers, R. M., J. E. Parkes, and M. A. Mantenieks (1992) "Multimegawatt MPD Thruster Design Considerations", in *Proc. Ninth Symposium on Space Nuclear Power Systems*, M. S. El-Genk and M. D. Hoover, eds., AIP Conference Proceedings 246, held in Albuquerque, NM, 12-16 January 1992.

Niewood, E. H., J. C. Preble, D. E. Hastings, and M. Martinez-Sanchez (1990) "Electrothermal and Modified Two Stream Instabilities in MPD Thrusters", AIAA 90-2607, July 1990.

Preble, J. C. (1990) Onset in Magnetoplasmadynamic Thrusters: A Model of an Electrothermal Instability, M.S. Thesis, Department of Aeronautics and Astronautics, Massachussetts Institute of Technology, Cambridge, MA, May 1990.

Randolph, T. M., W. F. von Jaskowsky, A. J. Kelly, and R. G. Jahn (1992) "Measurement of Ionization Levels in the Interelectrode Region of an MPD Thruster", AIAA 92-3460, July 1992.

Salhi, A. and P. J. Turchi (1992) "A First-Principles Model for Orificed Hollow Cathode Operation", AIAA 92-3742, July 1992.

Schroff, A. M., P. Palluel, and J. C. Tonnerre (1981) "Performance and Life Tests of Various Types of Impregnated Cathodes", *Applications of Surface Science*, **8** (1981):36-49.

Sovey, J. S. and M. A. Mantenieks (1988) "Performance and Lifetime Assessment of MPD Arc Thruster Technology", AIAA 88-3211, July 1988; also see NASA TM-101293, August 1988.

Stone, J. R. (1992) "Nuclear Electric Propulsion: An Integral Part of NASA's Nuclear Propulsion Project", in *Proc. Ninth Symposium on Space Nuclear Power Systems*, M. S. El-Genk and M. D. Hoover, eds., AIP Conference Proceedings 246, held in Albuquerque, NM, 12-16 January 1992.

Subramaniam, V. V. and J. L. Lawless (1988) "Electrode-Adjacent Boundary Layer Flow in Magnetoplasma-dynamic Thrusters", *Phys. Fluids*, 31(1): 201-209.

Tahara, H., H. Yaasui, Y. Kagaya, and T. Yoshikawa (1987) "Experimental and Theoretical Researches on Arc Structure in a Self-Field Thruster", AIAA 87-1093, May 1987.

Tilley, D. L. (1991) An Investigation of Microinstabilities in a kW Level Self-Field MPD Thruster, M.S. Thesis 1917-T, Department of Mechanical and Aerospace Engineering, Princeton University, Princeton, NJ, October 1991.

Wagner, H. P., M. Auweter-Kurtz, T. Roesgen, E. W. Messerschmid, and H. J. Kaeppeler (1990) "Gradient Driven Instabilities in Stationary MPD Thruster Flows", AIAA 90-2603.

REPORT DOCUMENTATION PAGE

Public reporting burden for this collection of information is estimated to average 1 hour per response, including the time for reviewing instructions, searching existing data sources, gathering and maintaining the data needed, and completing and reviewing the collection of information. Send comments regarding this burden estimate or any other aspect of this collection of information, including suggestions for reducing this burden, to Washington Headquarters Services, Directorate for information Operations and Reports, 1215 Jefferson Davis Highway, Suite 1204, Arlington, VA 22202-4302, and to the Office of Management and Budget, Paperwork Reduction Project (0704-0188), Washington, DC 20503.

1. AGENCY USE ONLY (Leave blank)	2. REPORT DATE	3. REPORT TYPE AND DATES COVERED
	January 1993	Final Contractor Report

4. TITLE AND SUBTITLE

Numerical Study of Cathode Emission Constraints on Cylindrical Self-Field MPD Thruster Performance

5. FUNDING NUMBERS

WU–506–42–31

6. AUTHOR(S)

Michael R. LaPointe

7. PERFORMING ORGANIZATION NAME(S) AND ADDRESS(ES)

Sverdrup Technology, Inc.
Lewis Research Center Group
2001 Aerospace Parkway
Brook Park, Ohio 44142

8. PERFORMING ORGANIZATION REPORT NUMBER

E–7416

9. SPONSORING/MONITORING AGENCY NAMES(S) AND ADDRESS(ES)

National Aeronautics and Space Administration
Lewis Research Center
Cleveland, Ohio 44135–3191

10. SPONSORING/MONITORING AGENCY REPORT NUMBER

NASA CR–190795

11. SUPPLEMENTARY NOTES

Prepared for the Tenth Symposium on Space Nuclear Power and Propulsion sponsored by the Institute for Space Nuclear Power Studies, Albuquerque, New Mexico, January 10–14, 1993. Project Manager, James S. Sovey, (216) 433–7454.

12a. DISTRIBUTION/AVAILABILITY STATEMENT

Unclassified - Unlimited
Subject Categories 20 and 64

12b. DISTRIBUTION CODE

13. ABSTRACT (Maximum 200 words)

A stability equation relating thruster discharge current, argon propellant mass flow rate, and electrode geometry has been solved for a variety of cylindrical self-field MPD thruster configurations and discharge currents. Realistic values for cathode emission current densities were used to provide additional constraints on the thruster geometries. A two-dimensional MPD code was employed to provide better estimates of the maximum achievable specific impulse, thrust, and flow efficiency for cases of interest. The model results indicate that long life, cylindrical self-field MPD thrusters operated with argon propellant may not be able to provide specific impulse values in excess of 2100 s. Alternate electrode geometries, applied magnetic fields, and/or low molecular weight propellants may be necessary to achieve higher values of specific impulse.

14. SUBJECT TERMS

MPD; Electric propulsion; Numerical simulation

15. NUMBER OF PAGES

14

16. PRICE CODE

A03

17. SECURITY CLASSIFICATION OF REPORT	18. SECURITY CLASSIFICATION OF THIS PAGE	19. SECURITY CLASSIFICATION OF ABSTRACT	20. LIMITATION OF ABSTRACT
Unclassified	Unclassified	Unclassified	